Hindawi
Journal of Engineering
Volume 2022, Article ID 9523767, 12 pages
https://doi.org/10.1155/2022/9523767

Research Article

Numerical Modeling of a Hot Plate Stove for Peanut Roasting

Anthony Agyei-Agyemang,[1] **Michael Kweku Commeh**,[2] **Peter Oppong Tawiah**,[1] **and Benjamin Atribawuni Asaaga**[1]

[1]*Department of Mechanical Engineering, College of Engineering, Kwame Nkrumah University of Science and Technology, Kumasi, Ghana*
[2]*Technology Consultancy Centre, College of Engineering, Kwame Nkrumah University of Science and Technology, Kumasi, Ghana*

Correspondence should be addressed to Anthony Agyei-Agyemang; tonyagyemang@yahoo.com

Received 7 June 2021; Revised 6 December 2021; Accepted 21 December 2021; Published 3 February 2022

Academic Editor: Elsa de Sá Caetano

Heat treatment, especially roasting, is known to reduce harmful fungal species and mycotoxin formation to a great extent. Experiments were conducted for heat treatment and the effects of introducing different fin configurations. ANSYS Fluent 14.5 was used to simulate the three-dimensional (3D) roaster geometry. The effect of the addition of different fins at the bottom of the hot plate was then studied. It was observed that maximum surface temperatures of 133°C, 153.25°C, 310.63°C, and 265.07°C were obtained after 180 minutes (three hours) for the experimental (without fins), predicted (without fins), predicted (with rod fins), and predicted (with honeycomb fins), respectively. The addition of honeycomb and rod fins to the roster's plate increased temperatures by 115.34% and 143.03% of the original roaster hot plate. Thus, a design with rod fins added to the hot plate could improve its thermal performance and hence reduce the harmful effects of possible fungal species and mycotoxin contamination.

1. Introduction

Peanut or groundnut (*Arachis hypogaea*) is a very valuable food crop and is mainly cultivated in the tropical and subtropical regions in Africa, America, and Asia [1]. The dry-roasted peanut kernels without salt are very rich in fatty acids (50%), proteins (25%), fiber, vitamin B6, vitamin E, niacin, and minerals. The minerals include manganese, magnesium, potassium, copper, and phosphorus [2]. Peanut is the richest nut in terms of protein and vitamin B3 (niacin) content [2], and it contains very high-quality oil. Its oil has a high smoke point and is, therefore, ideal for cooking or frying at high temperatures [2, 3].

Production of oil from peanuts involves the processing of groundnut by shelling, roasting, and pressing [4]. It is also used in making soap, cosmetics, furniture cream, shaving cream, fuel, and lubricants. Due to the fact that peanut is produced in the tropics where temperature and humidity are usually high, and also as a result of poor processing procedures, it is often associated with infestation with different species of fungus and formation of mycotoxins [5, 6]. Among these are aflatoxins (AFs), which are very dangerous to animal and human health [6, 7]. Heating can reduce the level of aflatoxin contamination in contaminated seeds, as revealed by different studies. Lee et al. [8] reported that the concentration of AFB_1 could be reduced by about 80% by roasting peanuts for 30 min at 150°C. This makes roasting as a peanut processing method very important. Roasting is very important for making different nut products [9]. The peanut roaster is used to process other nut products as well, which in the process results in the development of color, flavor, and texture of the final product through several complex chemical reactions, heat transfer, and drying processes [10]. Roasting should be given special attention since it is used to improve food safety, introduce desired flavor, color, and texture and to improve and preserve food crops like grains, cocoa, coffee, and peanuts [9, 11]. The process of roasting also makes processed foods, especially nuts, more palatable

and acceptable [12]. It has been observed that the improved taste, color, and texture of the processed food, and for that matter peanut, depend mainly on the roasting process [13].

Kita and Figiel [14] characterize roasting methods into two main groupings, namely, roasting in oil and dry roasting in air methods. Generally, the roasting process changes the microstructure of the nuts to develop the peculiar crunchy and crispy texture of the nuts and reduces the possible presence of poisonous fungi in peanut kernels and ultimately brings down the level of aflatoxins [15]. In dry roasting, two main methods are employed: the microwave and convection methods. The microwave roasting involves placing the peanut in a microwave oven and heating it for a few minutes [16]. In the convection method, peanuts are heated on a plate or by allowing air at a determined elevated temperature to flow at a given speed through the nuts to roast them [17]. Roasting on a heated plate is the most common method used in Ghana.

Proper roasting process is very important for the development of taste, color, and texture of the final product [13]. Lykomitros et al. [18] discovered that the flavor and color of roasted peanuts have a strong impact on consumer acceptance of the product. In a study to investigate the effect of different roasting methods of peanut on peanut color, flavor, and lipid oxidation values, Smith [19] did it for different time and temperature combinations using oven, microwave, and combination roasting technologies and observed that the method was not significant but rather the temperature and time of roasting were most essential.

Different time periods and temperatures are used to roast peanuts to obtain some specific product qualities for a specific market segment [16]. Specific time-temperature combinations used during peanut roasting have been observed to produce the same surface color [10]. It is, therefore, necessary to know the temperature-time combinations needed to roast for the best-desired peanut characteristics. Davids [20] reported a temperature-time combination of 240–275°C for the duration between 3 and 30 minutes, for some roasters. Raemy and Lambelet [21] found out that roasting starts as an endothermic reaction but later turns into an exothermic reaction at a roasting temperature of about 175°C, that is, the products being roasted heat themselves up in the process.

Some roasters are electrically powered but are mostly combined with an extractor [22]. This kind of combination makes the machines more complex and expensive for peanut vendors who are small-scale enterprises (SMEs). Peanut seeds are traditionally roasted by constantly stirring the groundnut seeds in an open mild steel pan over an open wood fire. Often, small open sand bath pan roasters, which are not efficient and hygienic, are used to roast the nuts [23]. Peanut, which indisputably is a valuable crop, is unfortunately associated with drudgery and bad hygiene in the developing world, which could be a source of physical and microbial contamination to the product [24]. This technique is rather hazardous and causes a great deal of discomfort to the operator due to constant contact with heat and smoke from the fire. Peanut processors who use this method need a roaster that would be user-friendly and easily maintained at a relatively lower cost. Therefore, this study proposes a groundnut roaster that is economical, efficient, and ergonomically suitable for SMEs that will be fueled with biofuel.

Biofuel, unfortunately, has its own demerits. Over 69% of the population in Africa use biomass as a traditional and most reliable fuel source of energy used for cooking. However, the effects of these demerits could be drastically reduced if more efficient and improved stoves are used. A study in India found that, if improved biomass cookstoves were widely accepted and implemented, it would have very significant benefits for health; for example, if theoretically 150 million cleaner burning improved biomass cookstoves were introduced and used over a period of ten years, about 2.2 million deaths could be avoided [25]. That is very significant. The hot plate roaster under study is an improved version of the traditional open mild steel pan over an open wood fire. This study considered the use of the computational fluid dynamics (CFD) approach to study the thermal performance of different fin configurations introduced in the hot plate roaster.

2. Experimental Setup

The hot plate stove consists of a brick structure, which is the main insulating material housing the roaster components. The rocket stove profile (cavity) from inlet (air and fuel) to outlet was designed and constructed using bricks. A stainless steel pan was fixed at the top of the brick structure to serve as a hot plate for the peanut roasting. Figure 1 shows a photograph of the roaster, while Figure 2 shows its CAD model. The roaster was equipped with a K-type thermocouple, which was used to measure the ambient, flame tip, and hot plate surface temperatures. The temperature measurement was taken at 5-minute intervals during the experiment. The K-type thermocouples have a temperature range from −200 to 1260°C and a sensitivity of 41 μV/°C. The flame tip and the hot plate surface temperatures were measured throughout the roasting period.

3. Computational Fluid Dynamics (CFD) Analysis

ANSYS Fluent 14.5 was used to simulate the three-dimensional (3D) stove geometry. The geometry was created in SpaceClaim 2020 R1 software as shown in Figure 2(a). The geometry was discretized into a finite volume mesh with 3.05×10^5 nodes and 1.14×10^6 elements. Figure 2(b) presents an image of the meshed volume. The fluid and component material properties that include air, brick, and stainless steel are shown in Table 1. These fluid and material properties were assigned to the model to describe the physical system (hot plate roaster) under consideration. The ANSYS Fluent solver was used for the numerical computations. The pressure-based solver, which represents an implicit solution approach that features the momentum and pressure correction as its primary variables, was used due to its unique applicability in solving a range of flow regimes ranging from low-speed incompressible flow to high-speed compressible flows, while expending less computer memory

Figure 1: Hot plate roaster.

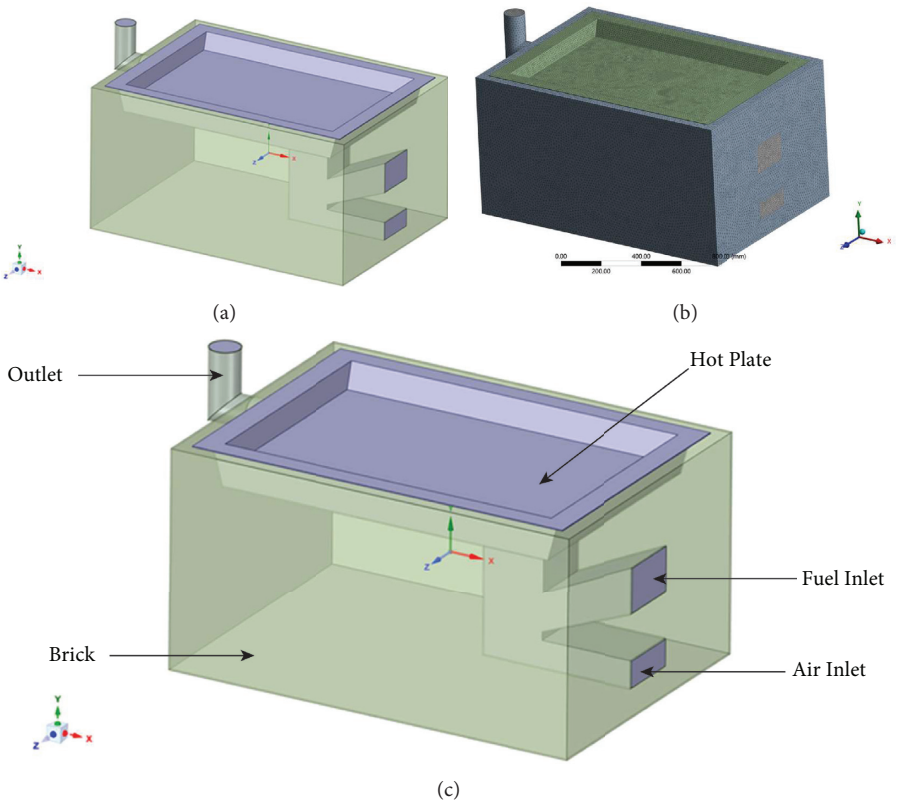

Figure 2: Hot plate roaster boundary specifications.

Table 1: Material properties of roaster components.

Material properties	Air	Brick	Stainless steel
Material type	Fluid	Solid	Solid
Density (kg/m^3)	1.225	2100	8030
Thermal conductivity (W/m^{-k})	0.0242	0.73	16.27
Specific heat (J/kg^{-k})	1006.43	850	502.48
Viscosity (kg/m^{-s})	1.7894e – 05	—	—

and storage. The model validation was carried out using the mean absolute error (MAE), Nash–Sutcliffe efficiency (NSE), root mean square error-to-observation standard deviation ratio (RSR), and the percent bias models to check the goodness of fit. This was performed by comparing the simulated results with the experimental results in accordance with the literature [26–31].

3.1. Boundary Conditions. Figure 2(c), Figure 3, and Tables 2 and 3 present the boundary condition assignment details and the flame tip input data used in the simulation. The flame tip temperature was measured using a K-type thermocouple from the roasters' combustion chamber and used as an input in the Fluent simulation. This was conducted in order to ensure that both experimental and numerical simulations had the same input conditions. The transient setting in the Fluent environment was selected, and the time-dependent temperature (flame tip temperature) of the flue gas was prepared as an input text file, which was imported into the Fluent environment. The inlet velocity of the flue gas was 0.3 m/s, and the ambient temperature was 30.1°C. As the flue gas rises, it flows beneath the hot plate and transfers heat to it by convection. The flue gas then moves toward the chimney and escapes into the environment. The walls of the hot plate roaster were assigned a no-slip boundary condition.

3.2. Constitutive CFD Model Setup. The governing equations of mass, momentum, and energy conservation of the heat transfer sequence were used to model, using the continuity, Navier-Stokes, and the energy equations, respectively. k and ε turbulent models were used in this study, where k is the turbulent kinetic energy and ε is the representation of the rate of dissipation. Equations (1)–(3) show the continuity, momentum, and the turbulent model equations used in this study:

Continuity equation:

$$\frac{\partial \rho}{\partial t} + \frac{\partial}{\partial x_i}\left(\rho u_i\right) = 0. \tag{1}$$

Momentum equation:

$$\frac{\partial\left(\rho u_i\right)}{\partial t} + \frac{\partial\left(\rho u_j u_i\right)}{\partial x_j} = -\frac{\partial p}{x_j} + \frac{\partial}{x_j}\left[\mu_{eff}\left(\frac{\partial u_i}{\partial x_j} + \frac{\partial u_j}{\partial x_i}\right)\right] - \rho g \delta_{3j}. \tag{2}$$

Here, effective viscosity is the sum of laminar viscosity and turbulence viscosity $\mu_{eff} = \mu_1 + \mu_t$. The gravity is active in negative z direction as the Kronecker delta operator δ_{3j} indicates.

Turbulence model:

The turbulence viscosity is given as follows:

$$\mu_t = \rho C_\mu \frac{k^2}{\varepsilon}, \tag{3}$$

where $C_\mu = 0.09$ (Launder and Spalding, 1974). k and ε are turbulence kinetic energy and turbulence kinetic energy dissipation rate, respectively [32–35].

4. Results and Discussion

4.1. Grid Independence and Convergence Tests. A mesh convergence and independence test depict computing a numerical solution on successively finer grids. The numerical results are improved by using successively smaller cell sizes for the computation. A grid independence test was carried out by varying the refined mesh element size from 25 mm to 10 mm for the hot plate stove model before carrying out the full-scale fluid simulation. All solutions converged for the various mesh sizes. The results presented in Figure 4 show an insignificant change in temperature after varying or reducing the element size from 20 mm to 10 mm. Results from Figure 4(a) indicate that the element sizes between 10 mm and 20 mm reached numerical stability, with no significant change in the hot plate surface temperature below a mesh size of 15 mm. The results from the element size of between 25 mm and 10 mm indicate that the appropriate definition and mesh refinement are essential in obtaining accurate numerical simulation results. Therefore, a mesh element size of 10 mm was chosen for the simulation.

4.2. Study of the Hot Plate Temperature. The surface temperatures of the hot plate are shown in Table 4 and Figure 5 for the experimental and predicted conditions. The surface temperature results present a maximum difference of 33.3°C after 95 minutes, a minimum difference of 0.00°C at the onset, and an average difference of 16.51°C. The surface temperatures for the two conditions attained maximum temperatures of 133.7°C and 143.847°C at the end of the roasting period (3 hours). The surface temperature difference (for both test conditions) at the end of the roasting period was about 10°C. Furthermore, the experimental and predicted test conditions presented in Figure 5 show very similar results (line patterns), which confirm the prediction capabilities of using the model and Fluent software. The results demonstrate that CFD can be used to improve cookstove design as it is cost-effective and allows several

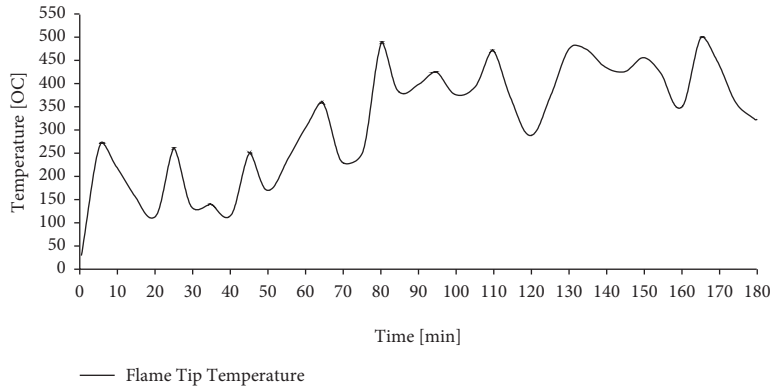

Figure 3: Time-dependent flame tip temperature.

Table 2: Boundary conditions used in the CFD simulation.

Part of the computational domain	Boundary condition	Boundary condition details
Inlet (flue gases from furnace)	Velocity inlet	The velocity of the air was 0.3 m/s. The ambient air temperature was 30.1°C, while the heated air from the combustion chamber (flame tip temperature) was measured and inputted from the experiment.
Outlet	Pressure outlet	The gauge pressure was assumed to be zero.
Hot plate	Wall	Stainless steel material was assigned to the hot plate.
Brick wall	Wall	The brick wall external temperature was assigned 30.1°C (which is the same as the ambient temperature).
Furnace internal wall	Wall	Brick material was assigned to the furnace internal walls.

Table 3: Time-dependent flame tip temperature.

No.	Time (min)	Flame tip temperature, °C	No.	Time (min)	Flame tip temperature, °C
1.	0	30.1	20.	95	428.2
2.	5	269	21.	100	379.9
3.	10	224	22.	105	396.2
4.	15	159.7	23.	110	475
5.	20	117.9	24	115	372.5
6.	25	264.9	25.	120	291.6
7.	30	137.5	26.	125	376.2
8.	35	143.4	27	130	478
9.	40	119.7	28	135	477
10.	45	253.6	29.	140	439.1
11.	50	173.5	30.	145	429
12.	55	238.7	31.	150	459.5
13.	60	310.1	32.	155	424.7
14.	65	360.7	33.	160	352
15.	70	234.2	34.	165	500.3
16.	75	255.1	35.	170	451.5
17.	80	490.2	36.	175	360.9
18	85	386.6	37.	180	325.5
19.	90	401.3		—	—

design iterations without the need of developing several physical models or prototypes.

4.3. Model Validation Results. The model validation was performed using the mean absolute error (MAE), Nash–Sutcliffe efficiency (NSE), root mean square error-to-observation standard deviation ratio (RSR), and the percent bias (PBIAS) models to check the goodness of fit. This was performed by comparing the simulated results with the experimental results:

The mean absolute error (MAE): MAE as given in equation (4), which gives how closely the observed and modeled datasets agree. It evaluates the magnitudes of the deviations of modeled datasets from the observed

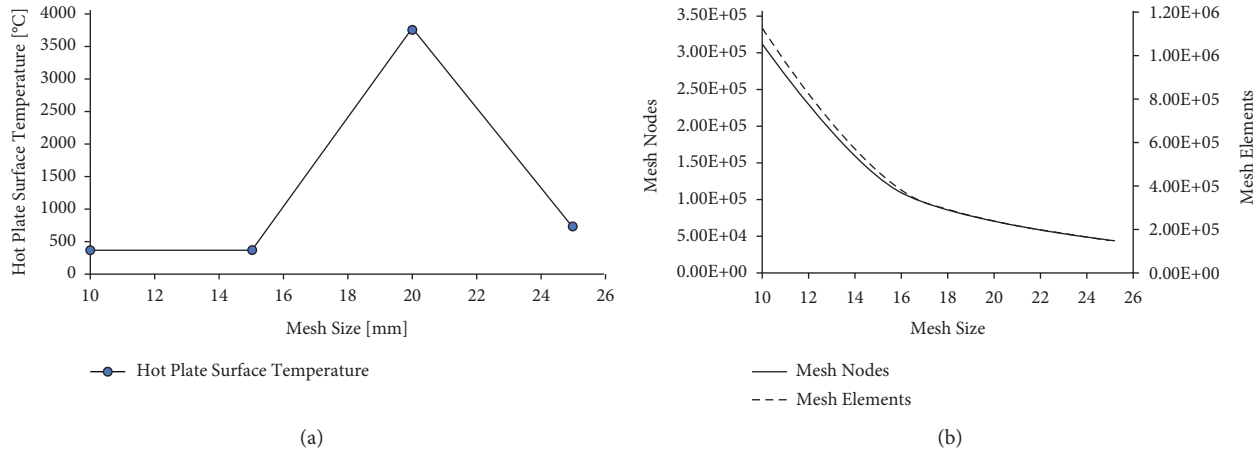

Figure 4: Grid independence test.

Table 4: Hot plate surface temperature versus time.

No.	Time (min)	Experimental (°C)	Predicted (°C)	No.	Time (min)	Experimental (°C)	Predicted (°C)
1	0	30.1	30.1	20	95	110	143.3
2	5	42.3	50.8	21	100	110.9	142.1
3	10	47.0	67.2	22	105	115.3	141.5
4	15	57.4	70.7	23	110	120.6	148.1
5	20	55.3	69.3	24	115	118.4	144.8
6	25	64.1	78.5	25	120	111.7	133.90
7	30	66.7	78.0	26	125	121.3	132.5
8	35	69.3	75.4	27	130	126.1	142.2
9	40	66.3	71.1	28	135	129.5	150.4
10	45	79.0	79.2	29	140	131.1	152.6
11	50	76.3	81.1	30	145	124.4	152.0
12	55	78.2	86.4	31	150	133	153.2
13	60	83.2	97.5	32	155	131.5	151.8
14	65	90.4	110.9	33	160	128.4	144.0
15	70	88.9	109.6	34	165	135.5	150.2
16	75	83.7	107.4	35	170	138	154.4
17	80	101.1	126.4	36	175	135.4	149.9
18	85	107.4	134.9	37	180	133.7	143.9
19	90	108.7	139.0	—	—	—	

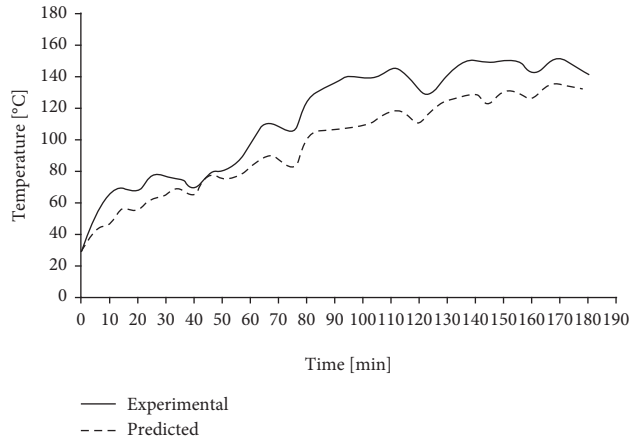

Figure 5: Hot plate surface temperature for the experimental and predicted conditions.

Table 5: Error interpretation.

Error type	Value
NSE	0.5976
MAE	17.4048
RSR	0.4024
PBIAS	−17.6423

values in real units, irrespective of the magnitude of the event [36].

$$\mathrm{MAE} = \frac{1}{n}\sum_{i=1}^{n}\left|\left(Y^{obs} - Y^{sim}\right)\right|, \tag{4}$$

where n = samples used; Y^{obs} = measured parameter (from observation); and Y^{sim} = calculated parameter (from simulation).

The root mean square error (RMSE)-to-observation standard deviation ratio (RSR): RSR uses error index statistics and a scaling/normalization factor and, therefore, makes it possible for the statistic and reported values from it to apply different parameters. RSR values range from zero (0) to a large positive value. The optimum value is zero (0), which indicates a perfect simulation model. Equation (5) gives the mathematical formula for RSR [37].

$$\mathrm{RSR} = \frac{\mathrm{RMSE}}{\mathrm{STDEV}_{obs}} = \frac{\left[\sqrt{\sum_{i=1}^{n}\left(Y_i^{obs} - Y_i^{sim}\right)^2}\right]}{\left[\sqrt{\sum_{i=1}^{n}\left(Y_i^{obs} - Y^{mean}\right)^2}\right]}, \tag{5}$$

where $Y_i^{obs} = i$th observation; $Y_i^{sim} = i$th simulated value; Y^{mean} = mean of observed data; and n = total number of observations.

Nash–Sutcliffe Efficiency (NSE): the Nash–Sutcliffe efficiency (NSE) is a normalized statistic that gives a comparison of the magnitude of the residual variance (the "noise") to the measured data variance (the "information") [38]. NSE can be mathematically represented by the following equation:

$$\mathrm{NSE} = 1 - \left[\frac{\sum_{i=1}^{n}\left(Y_i^{obs} - Y_i^{sim}\right)^2}{\sum_{i=1}^{n}\left(Y_i^{obs} - Y^{mean}\right)^2}\right], \tag{6}$$

where $Y_i^{obs} = i$th observation; $Y_i^{sim} = i$th simulated value; Y^{mean} = mean of observed data; and n = total number of observations.

Percent Bias (PBIAS): percent bias (PBIAS) represents the tendency of the simulated data to be larger or smaller than their observed data as a percentage [39]. 0.0 is the optimal value of PBIAS. Lower values of the magnitude show that the accuracy of the model simulation is better. PBIAS is mathematically represented by the following equtaion:

$$\mathrm{PBIAS} = \left[\frac{\sum_{\mathrm{i}=1}^{\mathrm{n}}\left(Y_{\mathrm{i}}^{\mathrm{obs}} - Y_{\mathrm{i}}^{\mathrm{sim}}\right)\times(100)}{\sum_{\mathrm{i}=1}^{\mathrm{n}}\left(Y_{\mathrm{i}}^{\mathrm{obs}}\right)}\right], \tag{7}$$

where $Y_i^{obs} = i$th observation; $Y_i^{sim} = i$th simulated value; and n = total number of observations.

The mean absolute error (MAE) value for the study was 17.4048, indicating an error of about 17.4°C. The Nash–Sutcliffe efficiency (NSE) value was 0.5976, which from Table 5 indicates that the simulated model just satisfactorily fits the experimental data, since NSE is an indicator of how well the plot of observed versus simulated data fits. The RMSE-to-observation standard deviation ratio (RSR) value was 0.4024, showing that the model simulation performance was very good. The percent bias (PBIAS) value was −17.6423. Negative values of PBIAS indicate model overestimation bias. From Table 6, the PBIAS value shows that the accuracy of the model simulation was only satisfactory. RSR, NSE, and PBIAS results show that the use of the CFD modeling approach is good and can be effectively used to model and conduct design improvements for roasters.

4.4. Thermal Performance Analysis of the Hot Plate Roaster Model with Different Heat Exchange (Fins) Configurations. In this section, the effect of the addition of fins to improve the thermal performance of the hot plate was analyzed. The hot plate was modified to include two different fin configurations. These fin configurations are rod (12.7 mm diameter) and honeycomb (made with 2 mm thick steel plate) as shown in Figure 6. Tables 7 and 6 present the surface temperatures for the experimental and predicted conditions with different fin configurations. The results show a maximum surface temperatures of 133°C, 153.25°C, 310.63°C, and 265.07°C after 180 minutes (three hours) for experimental (without fins), predicted (without fins), predicted (with rod fins), and predicted (with honeycomb fins), respectively. The average hot plate surface temperature results for experimental (without fins), predicted (without fins), predicted (with rod fins), and predicted (with honeycomb fins) were 93.1°C, 111.0°C, 169.64°C, and 139.46°C, respectively. From the presented results, the addition of fins to the hot plate leads to a significant increase in temperature with a maximum difference of 132.07°C and 177.63°C for predicted (hot plate with honeycomb fins) and predicted (hot plate with rod fins), respectively. Higher hot plate surface temperatures are desirable as it reduces the level of aflatoxin contamination in contaminated seeds [8]. Rod fins attained higher temperatures than honeycomb fins, which may be attributed to the high level of obstructions (in the honeycomb cells), which produced a temperature gradient leading to a reduction in heat transfer during the flow of the hot flue gases [40]. Figures 7 and 8 show the geometric models and temperature contour plots of the hot plate fin configurations (original plate without fins, hot plate with honeycomb fins, and hot plate with rod fins). The development of the cookstove prototype with the analyzed fins is recommended to validate the numerical results. There were 115.34% and 143.03% increase in hot plate surface temperatures for the honeycomb and rod fin modified hot plates over the original roaster, which is in agreement with Shashidhar's [41] findings. Thus, honeycomb and rod fins can be introduced to increase the thermal performance of the roaster plate.

Table 6: Validation statistics.

Performance rating	RSR	NSE	PBIAS
Very good	$0 \le RSR \le 0.5$	$0.75 < NSE \le 1$	PBIAS $< \pm 10$
Good	$0.5 < RSR \le 0.6$	$0.65 < NSE \le 0.75$	$\pm \le 10$ PBIAS $< \pm 15$
Satisfactory	$0.6 < RSR \le 0.7$	$0.5 < NSE \le 0.65$	$\pm 15 \le PBIAS < \pm 25$
Unsatisfactory	$RSR > 0.7$	$NSE \le 0.5$	$PBIAS > \pm 25$

Source: [31].

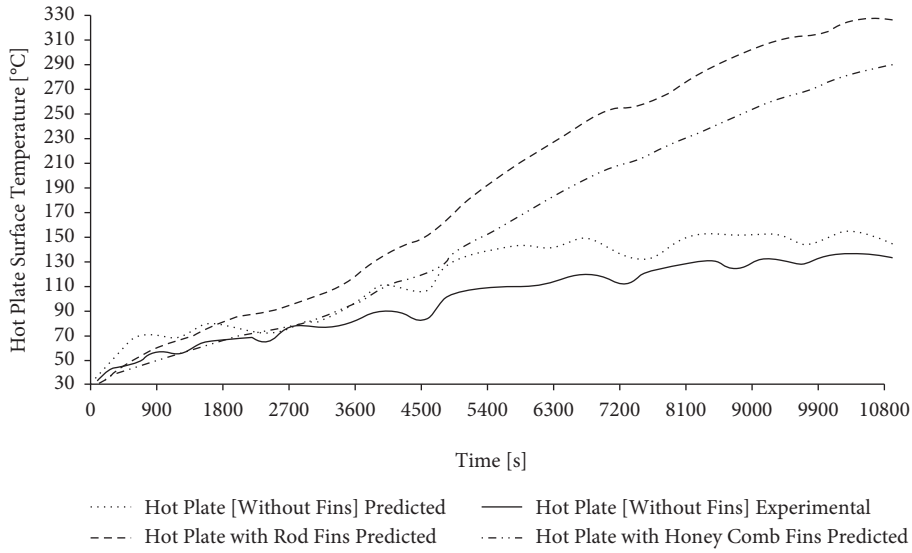

Figure 6: Hot plate surface temperature for the experimental and predicted conditions at different fin configurations.

Table 7: Hot plate surface temperature for the experimental and predicted conditions at different fin configurations versus time.

Time (s)	Hot plate surface temperature			
	Hot plate (without fins) experimental (°C)	Hot plate (without fins) predicted (°C)	Hot plate with rod fins predicted (°C)	Hot plate with honeycomb fins predicted (°C)
0	30.1	30.1	30.1	30.1
300	42.3	50.83688	40.52949	37.42657
600	47	67.20928	53.49955	45.85424
900	57.4	70.70168	62.17645	51.75321
1200	55.3	69.30462	67.21052	55.5708
1500	64.1	78.50634	76.67537	62.32829
1800	66.7	78.10656	83.56199	67.47927
2100	69.3	75.38275	87.29558	70.79904
2400	66.3	70.98046	89.95532	73.46316
2700	79	79.12975	97.17179	79.0695
3000	76.3	81.09478	103.7069	84.29769
3300	78.2	86.40991	110.8094	90.05375
3600	83.2	97.53341	121.8798	98.34925
3900	90.4	110.9372	135.6838	108.5371
4200	88.9	109.6522	144.5668	115.765
4500	83.7	107.1539	151.1753	121.7142
4800	101.1	126.4397	167.0472	133.6128
5100	107.4	134.8871	182.9843	145.6897
5400	108.7	138.9646	196.2829	156.3919
5700	110	143.3	209.8445	167.4088
6000	110.9	142.1373	221.0136	177.0444
6300	115.3	141.5335	231.034	186.078
6600	120.6	148.1008	243.6005	196.81
6900	118.4	144.8226	252.6613	205.347

Table 7: Continued.

Time (s)	Hot plate surface temperature			
	Hot plate (without fins) experimental (°C)	Hot plate (without fins) predicted (°C)	Hot plate with rod fins predicted (°C)	Hot plate with honeycomb fins predicted (°C)
7200	111.7	133.9076	255.5703	209.997
7500	121.3	132.4922	259.7463	215.5144
7800	126.1	142.2089	269.4999	224.5233
8100	129.5	150.4031	280.9035	234.5581
8400	131.1	152.6216	289.9701	243.198
8700	124.4	151.9939	297.073	250.6639
9000	133	153.2493	304.587	258.3506
9300	131.5	151.835	310.6253	265.0674
9600	128.4	143.9568	312.6161	269.2107
9900	135.5	150.2267	318.7322	275.9133
10200	138	154.3543	325.557	282.9557
10500	135.4	149.8572	327.0896	286.6313
10800	133.7	143.8465	324.9341	287.9087

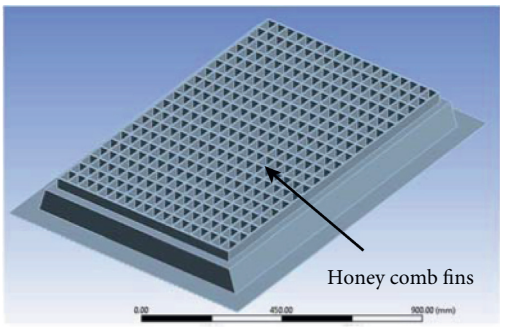

Honey comb fin modification

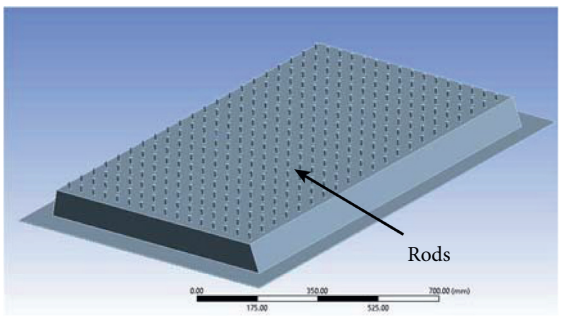

Rod fin modification

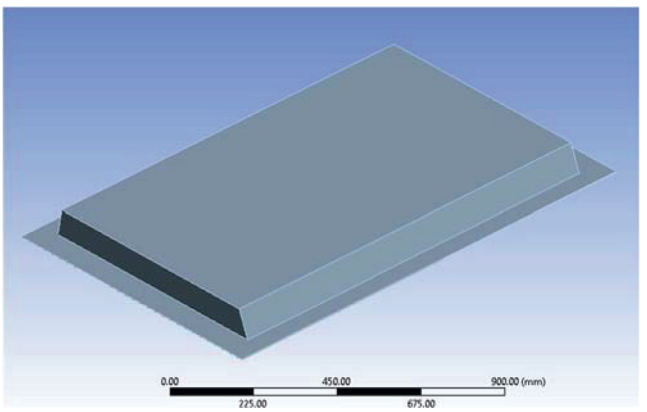

Original design

Figure 7: Hot plate surface geometric models with design modification (different fin configurations).

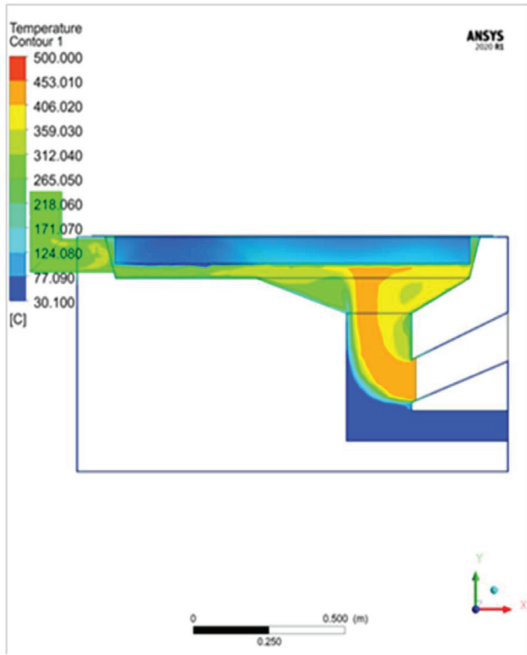

Original design

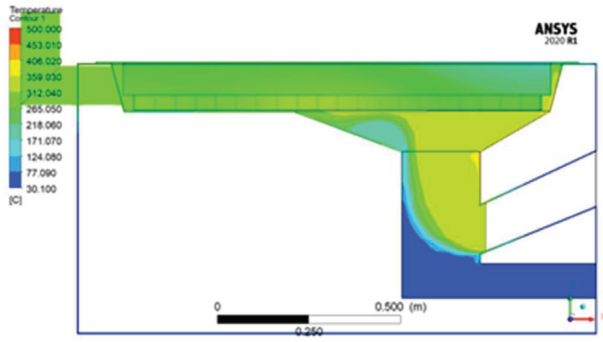

Honey comb fin modification

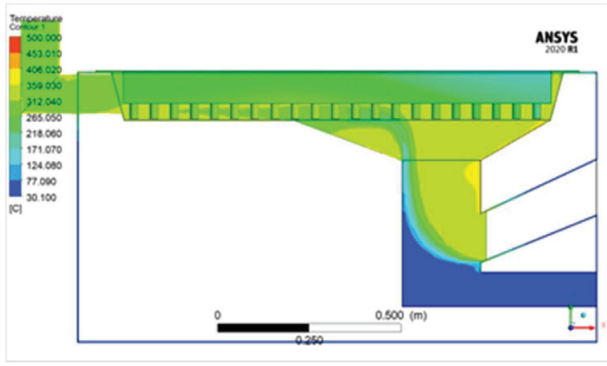

Rod fin modification

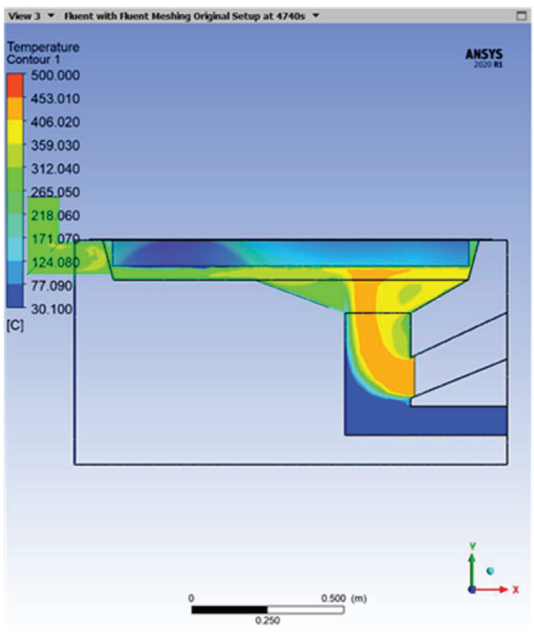

Original design

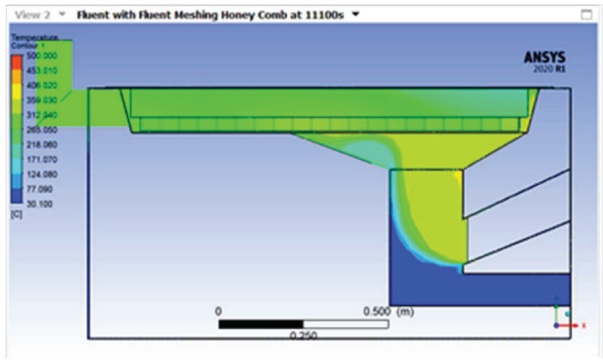

Honey comb fin modification

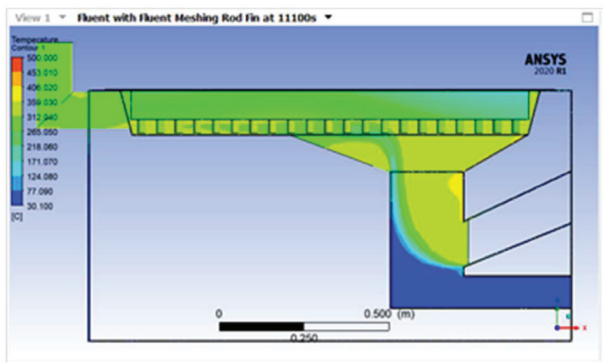

Rod fin modification

FIGURE 8: Temperature contour plot of a hot plate with different fin configurations (original plate without fins, hot plate with honeycomb fins, and hot plate with rod fins).

5. Conclusions

CFD simulation was used to analyze a biomass-fueled peanut roaster to improve its effectiveness and propose design improvement to reduce the harmful effects of biomass-powered stoves. The K-type thermocouple was used to measure the ambient, flame tip, and hot plate surface temperatures during the experiment at 5-minute interval during the experiment. ANSYS Fluent 14.5 was used to simulate the three-dimensional (3D) stove geometry. The experimental results were compared with the simulated results. Model validation was carried out using the mean absolute error (MAE), Nash–Sutcliffe efficiency (NSE), root mean square error-to-observation standard deviation ratio (RSR), and the percent bias (PBIAS) models to check the goodness of fit. The model fitted the experimental data well.

The effect of the addition of fins at the bottom of the hot plate to improve its thermal performance was studied. For the two (2) different fin configurations studied, i.e., rod (12.7 mm diameter) and honeycomb (made with 2 mm thick steel plate), maximum surface temperatures of 133°C, 153.25°C, 310.63°C, and 265.07°C were obtained after 180 minutes (three hours) for experimental (without fins), predicted (without fins), predicted (with rod fins), and predicted (with honeycomb fins), respectively. The results show that the addition of rod fins to the hot plate leads to the highest temperature. The introduction of honeycomb and rod fins on the roster plate increased temperatures by 115.34% and 143.03% of the original roaster hot plate temperature, which can drastically reduce the possible aflatoxin contamination effect. Thus, a design with rod fins added to the hot plate could improve its thermal performance and hence reduce harmful effects of the burning of its biofuels in support of the United Nations' Sustainable Development Goals (SDGs) 3, 7, 12, and 13.

Data Availability

The data gathered and used in this study are privately kept at the laboratory of the authors and can be made available upon request.

Conflicts of Interest

The authors declare that there are no conflicts of interest regarding the publication of this paper.

Authors' Contributions

Michael Kweku Commeh took part in the design of the roaster. Anthony Agyei-Agyemang, Michael Kweku Commeh, and Benjamin Atribawuni Asaaga carried out the experiments. Anthony Agyei-Agyemang and Benjamin Atribawuni Asaaga carried out the modeling work. Anthony Agyei-Agyemang and Benjamin Atribawuni Asaaga were involved in the data analysis. Peter Oppong Tawiah played a supervisory role and was also involved in editing.

Acknowledgments

The authors express their sincere appreciation to the Technology Consultancy Centre of the Kwame Nkrumah University of Science and Technology for allowing us to carry out the experimental works on their hot plate stove.

References

[1] N. A. Akram, F. Shafiq, and M. Ashraf, "Peanut (*Arachis hypogaea* L.): a prospective legume crop to offer multiple health benefits under changing climate," *Comprehensive Reviews in Food Science and Food Safety*, vol. 17, no. 5, pp. 1325–1338, 2018.

[2] International Nut & Dried Fruit Council, *Nuts & Dried Fruits - Statistical Yearbook 2019-2020*, International Nut & Dried Fruit Council, Dubai, United Arab Emirates, 2020.

[3] R. D. O'Brien: Fats and Oils: Formulating and Processing for Applications. 2004.

[4] A. Mohammed and A. B. Hassan, "Design and evaluation of a motorized and manually operated groundnut shelling machine," *International Journal of Emerging Trends in Engineering and Development*, vol. 4, no. 2, pp. 673–682, 2012.

[5] S. S. M. Reza, A. Masoud, T. Ali, G. Faranak, and N. Mahboob, "Determination of aflatoxins in nuts of Tabriz confectionaries by ELISA and HPLC methods," *Advanced Pharmaceutical Bulletin*, vol. 2, 2012.

[6] N. Chiewchan, A. S. Mujumdar, and S. Devahastin, "Application of drying technology to control aflatoxins in foods and feeds: a review," *Drying Technology*, vol. 33, no. 14, pp. 1700–1707, 2015.

[7] L. M. Martins, A. S. Sant'Ana, M. H. P. Fungaro et al., "The biodiversity of Aspergillus section Flavi and aflatoxins in the Brazilian peanut production chain," *Food Research International*, vol. 94, pp. 101–107, 2017.

[8] L. S. Lee, A. F. Cucullu, and L. A. Goldblatt, "Appearance and aflatoxin content of raw and dry roasted peanut kernels," *Food Technology*, vol. 22, pp. 1131–1134, 1968.

[9] A. Shakerardekani, R. Karim, H. M. Ghazali, and N. L. Chin, "Effect of roasting conditions on hardness, moisture content and colour of pistachio kernels," *SSRN Electronic Journal*, vol. 18, 2011.

[10] K. A. McDaniel, B. L. White, L. L. Dean, T. H. Sanders, and J. P. Davis, "Compositional and mechanical properties of peanuts roasted to equivalent colors using different time/temperature combinations," *Journal of Food Science*, vol. 77, no. 12, pp. C1293–C1299, 2012.

[11] M. van Boekel, V. Fogliano, N. Pellegrini et al., "A review on the beneficial aspects of food processing," *Molecular Nutrition & Food Research*, vol. 54, no. 9, pp. 1215–1247, 2010.

[12] P. Pittia, M. Dalla Rosa, and C. R. Lerici, "Textural changes of coffee beans as affected by roasting conditions," *Lebensmittel-Wissenschaft und -Technologie- Food Science and Technology*, vol. 34, no. 3, pp. 168–175, 2001.

[13] S. Ng, O. Lasekan, K. Muhammad, R. Sulaiman, and N. Hussain, "Effect of roasting conditions on color development and Fourier transform infrared spectroscopy (FTIR-ATR) analysis of Malaysian-grown tropical almond nuts (*Terminalia catappa* L.)," *Chemistry Central Journal*, vol. 8, no. 1, 2014.

[14] A. Kita and A. Figiel, "Effect of roasting on properties of walnuts," *Polish Journal of Food and Nutrition Sciences*, vol. 57, 2007.

[15] B. M. Ogunsanwo, O. O. P. Faboya, O. R. Idowu, O. S. Lawal, and S. A. Bankole, "Effect of roasting on the aflatoxin contents of Nigerian peanut seeds," *African Journal of Biotechnology*, vol. 3, no. 9, pp. 451–455, 2004.

[16] G. F. Opoku, *Process and Product Optimization and Storage Characteristics of Canned Peanut Soup Base*, University of Ghana, Accra, Ghana, 2013.

[17] J. N. Maduako, M. Saidu, P. Matthias, and I. Vanke, "Testing of an engine-powered groundnut shelling machine," *Journal of Agricultural Engineering*, vol. 14, pp. 29–37, 2006.

[18] D. Lykomitros, V. Fogliano, and E. Capuano, "Flavor of roasted peanuts (*Arachis hypogaea*)-part I: effect of raw material and processing technology on flavor, color and fatty acid composition of peanuts," *Food Research International*, vol. 89, pp. 860–869, 2016.

[19] A. L. Smith, *Evaluation of Peanut Roasting Using Oven and Microwave Technologies on the Development of Color, Flavor, and Lipid Oxidation*, The Ohio State University, Columbus, OH, USA, 2014.

[20] K. Davids, *Home Coffee Roasting, Revised*, Romance and revival. Macmillan, Harmondsworth, UK, 2003.

[21] A. Raemy and P. Lambelet, "A calorimetric study of self-heating in coffee and chicory," *International Journal of Food Science and Technology*, vol. 17, no. 4, pp. 451–460, 1982.

[22] O. J. Okegbile, A. B. Hassan, A. Mohammed, and O. Obajulu, "Design of a combined groundnut roaster and oil expeller machine," *International Journal of Science and Engineering Investigations*, vol. 3, no. 26, 2014.

[23] O. B. Olatunde, E. A. Ajav, and S. O. Fatukasi, "Design and fabrication of groundnut (*Arachis hypogaea*) roaster cum expeller," *International Journal of Science and Technology*, vol. 3, no. 3, pp. 177–184, 2014.

[24] A. Adeyinka Idowu, A. Olamide Abigael, A. Babatunde Kazeem, and O. Modupe Beatrice, "Design, fabrication and evaluation of electrically-operated groundnut roasting machine," *American Journal of Engineering and Technology Management*, vol. 5, no. 3, p. 48, 2020.

[25] P. Wilkinson, K. R. Smith, and M. Davies, "Public health benefits of strategies to reduce greenhouse-gas emissions: household energy," *Lancet*, vol. 374, pp. 1917–29, 2009.

[26] A. Ritter and R. Muñoz-Carpena, "Performance evaluation of hydrological models: statistical significance for reducing subjectivity in goodness-of-fit assessments," *Journal of Hydrology*, vol. 480, pp. 33–45, 2013.

[27] T. W. Chu, A. Shirmohammadi, and H. Montas, "Evaluation of the swat model's sediment and nutrient components in the piedmont physiographic region of Maryland," *Transactions of the ASAE*, vol. 47, no. 5, pp. 1523–1538, 2004.

[28] J. Singh, H. V. Knapp, J. G. Arnold, and M. Demissie, "Hydrological modeling OF the iroquois river watershed using HSPF and swat," *Journal of the American Water Resources Association*, vol. 41, no. 2, pp. 343–360, 2005.

[29] G. G. Vazquez-Amábile and B. A. Engel, "Use of SWAT to compute groundwater table depth and streamflow in the Muscatatuck River watershed," vol. 48, no. 3, pp. 991–1003, 2005.

[30] C. Willmott and K. Matsuura, "Advantages of the mean absolute error (MAE) over the root mean square error (RMSE) in assessing average model performance," *Climate Research*, vol. 30, no. 1, pp. 79–82, 2005.

[31] D. N. Arnold, M. W. Van Liew, R. L. Bingner, R. D. Harmel, and T. L. Veith, "Model evaluation guidelines for systematic quantification of accuracy in watershed simulations," *Transactions of the ASABE*, vol. 50, no. 3, pp. 885–900, 2007.

[32] A. Fluent Usa, "Ansys Fluent Theory Guide," 2011.

[33] B. E. Launder and D. B. Spalding, "The numerical computation of turbulent flows," *Computer Methods in Applied Mechanics and Engineering*, vol. 3, no. 2, pp. 269–289, □ 1974.

[34] B. E. Launder and D. B. Spalding, *Mathematical Models of Turbulence*, BOOK. Academic Press, Cambridge, MA, USA, 1972.

[35] B. E. Launder and D. B. Spalding, "The numerical computation of turbulent flows," in *Numerical Prediction of Flow, Heat Transfer, Turbulence and Combustion*Elsevier, Amsterdam, Netherlands, 1983.

[36] C. W. Dawson, R. J. Abrahart, and L. M. See, "HydroTest: a web-based toolbox of evaluation metrics for the standardised assessment of hydrological forecasts," *Environmental Modelling & Software*, vol. 22, no. 7, pp. 1034–1052, 2007.

[37] D. R. Legates and G. J. McCabe, "Evaluating the use of "goodness-of-fit" Measures in hydrologic and hydroclimatic model validation," *Water Resources Research*, vol. 35, no. 1, pp. 233–241, 1999.

[38] J. E. Nash and J. V. Sutcliffe, "River flow forecasting through conceptual models part I-a discussion of principles," *Journal of Hydrology*, vol. 10, no. 3, pp. 282–290, 1970.

[39] H. V. Gupta, S. Sorooshian, and P. O. Yapo, "Status of automatic calibration for hydrologic models: comparison with multilevel expert calibration," *Journal of Hydrologic Engineering*, vol. 4, no. 2, pp. 135–143, 1999.

[40] P. Gateau and P. Namy, "Comparison between honeycomb and fin heat exchangers," in *Proceedings of the Comsol Conference*, Boston, MA, USA, February 2011.

[41] V. V. Shashidhar, "Effect of using fins in cooking vessel to improve heat transfer rate," *AIP Publishing LLC*, vol. 2236, no. 1, p. 030008, 2020.